J. Fluid Mech. (2009), *vol.* 640, *pp.* 507–536.
doi:10.1017/S0022112009992011

A DNS study of effects of particle–particle collisions and two-way coupling on particle deposition and phasic fluctuations

HOJJAT NASR[1], GOODARZ AHMADI[1]† AND JOHN B. MCLAUGHLIN[2]

[1]Department of Mechanical and Aeronautical Engineering, Clarkson University, Potsdam, NY 13699-5725, USA

[2]Department of Chemical and Biomolecular Engineering, Clarkson University, Potsdam, NY 13699-5725, USA

(Received 4 November 2007; revised 5 September 2009; accepted 7 September 2009; first published online 13 November 2009)

This study is concerned with the effects of particle–particle collisions and the two-way coupling on the dispersed and carrier phase turbulence fluctuations in a channel flow. The time history of the instantaneous turbulent velocity vector was generated by the two-way coupled direct numerical simulation of the Navier–Stokes equations via a pseudo-spectral method. The particle equation of motion included the wall-corrected nonlinear drag force and the wall-induced and shear-induced lift force. The effect of particles on the flow was included in the analysis via a feedback force that acted on the computational grid points. Several simulations for different particle relaxation times and particle mass loadings were performed, and the effects of particle–particle collisions, particle feedback force and inter-particle interactions on the particle deposition velocity, fluid and particle fluctuating velocities, and particle concentration profiles were determined. The effect of particle aerodynamic interactions was also examined for certain cases.

The simulation results indicated that when particle–particle collisions were included in the computation but two-way coupling effects were ignored, the particle normal fluctuating velocity increased in the wall region causing an increase in the particle deposition velocity. When the particle collisions were neglected but the particle–fluid two-way coupling effects were accounted for, the two-way coupling and the particle normal fluctuating velocity decreased near the wall causing a decrease in the particle deposition velocity. In the case of the four-way coupling in which both inter-particle collisions and two-way coupling effects were present, it was found that the particle deposition velocity increased compared with the one-way coupling case. When the particle aerodynamic interactions were added to the four-way coupled case (termed six-way coupled case), no significant changes in the mean fluid and particle velocities and the fluid and particle fluctuating velocities were obtained.

The results for the particle concentration profile indicated that the inclusion of two-way coupling or inter-particle collisions into the computation reduced the accumulation of particles near the wall. It was also observed that particle–particle collisions and two-way coupling weakened the preferential distribution of particles.

Key words: multiphase and particle-laden flows, particle/fluid flows, turbulent flows

† Email address for correspondence: ahmadi@clarkson.edu

1. Introduction

The study of transport and deposition of aerosols in particle-laden flows is of considerable interest due to its importance in numerous industrial and environmental applications. Despite numerous experimental and computational studies, the interaction of particles with turbulence eddies is not fully understood. In particular, for non-dilute flows, the effect of the two-way coupling and particle collisions on turbulence modulation and particle transport and deposition are far from being understood.

The earliest model for turbulent deposition was reported by Friedlander & Johnstone (1957). They proposed the so-called free-flight theory, which implies that particles reaching the stopping distance from the wall will deposit on the wall. While this model gives relatively reasonable results for the eddy impaction regime, some of the assumptions of the free-flight model are difficult to justify. Caporaloni *et al.* (1975) and Reeks (1983) discussed the concept of turbophoresis. They showed that, due to spatial inhomogeneity of the turbulent intensities, there is a mean flux of particles towards the wall. Direct numerical simulations (DNS) of particle deposition in a turbulent channel flow were performed by McLaughlin (1989). He found that the Saffman lift force had a significant effect on aerosol deposition although the assumptions of Saffman's theory were not satisfied by many of the aerosols in the near-wall region. The simulation results of Wang & Stock (1993) showed the importance of nonlinear drag for particles with high settling velocities. Squires & Eaton (1991*a*) simulated a homogeneous isotropic non-decaying turbulent flow field by imposing an excitation at low wavenumbers and studied the effects of inertia on particle dispersion. They also used DNS to study the preferential micro-concentration structure of particles as a function of Stokes number in turbulent near-wall flows (Squires & Eaton 1991*b*). Ounis, Ahmadi & McLaughlin (1991, 1993) used DNS to study particle deposition in wall-bounded turbulent flows. They showed that the particle deposition process is mainly controlled by the near flow structures. Brooke *et al.* (1992) employed DNS to study particle deposition in a channel flow with the view of evaluating the free-flight theory of Friedlander & Johnstone (1957). Wang & Squires (1996) studied particle transport in fully developed turbulent channel flows using the one-way coupled large eddy simulations (LES) simulation. They showed that the LES technique accurately predicted that the value of the streamwise fluctuating velocity of the particles was larger than that of the fluid. Zhang & Ahmadi (2000) used DNS to study aerosol particle transport and deposition in vertical and horizontal turbulent duct flows. They showed that the wall coherent structure plays an important role in the particle deposition process. Marchioli & Soldati (2002) studied the behaviour of particles in the wall region of a turbulent channel flow using one-way coupled DNS. They found that the particle transfer mechanisms are strongly affected by turbulence bursts in the wall region. Narayanan *et al.* (2003) studied particle dispersion and deposition in a fully developed turbulent open channel flow using the DNS technique under the one-way coupling assumption. They showed that particles with non-dimensional relaxation times of 5 and 15 were strongly concentrated near the wall in the form of streamwise streaky structures. They also reported that the locations of the deposited small particle formed streamwise streaky patterns, while the larger (free-flight) particles randomly deposited on the wall. Arcen, Taniére & Oesterle (2006) used DNS and studied the importance of using the lift force and wall corrections of the drag coefficient for tracking solid particles in a fully developed channel flow. They showed that the lift force and the drag corrections do not lead to noticeable changes in the statistical properties of the solid particle distributions.

As particle mass loading increases, the effects of particles on the flow are no longer negligible. Hetsroni & Sokolov (1971) used hot-wire anemometry (HWA) to measure the modification of the turbulence intensity and energy spectra at different mass loadings of small droplets in a horizontal jet. They found that turbulence intensity decreased almost proportionally to droplet loading. Levy & Lockwood (1981) used Laser–Doppler anemometry (LDA) to measure the effect of sand particles on a downward jet. They found that particles smaller than 250 μm attenuated turbulence, while particles larger than 850 μm enhanced turbulence intensity. The first detailed measurements in a pipe flow were reported by Tsuji & Morikawa (1982). They used plastic particles with diameters of 200 μm and 3.4 mm in a horizontal pipe and reported a flattening of the mean fluid velocity profiles. They also found that large particles tended to increase turbulence intensity and small particles tended to decrease it. Tsuji, Morikawa & Shiomi (1984) conducted a similar experiment in a vertical pipe flow. In addition to the known trends of turbulence modifications by large and small particles, they also found that the medium-size particles increased turbulence in the pipe core region and decreased it near the walls.

Rashidi, Hetsroni & Banerjee (1990) performed an experimental study of particle–turbulence interactions near a wall, and found that the near-wall particle transport was mainly controlled by the turbulence burst phenomena. They also showed that the larger polystyrene particles (with a diameter of 1100 μm) increased the number of wall ejections and augmented the fluid turbulence, while the smaller polystyrene particles (with a diameter of 120 μm) caused a decrease in the number of wall ejections and attenuated the fluid turbulence.

Squires & Eaton (1990) studied the particle–turbulence interaction in a DNS of a fully turbulent homogenous flow. They found that the decrease of turbulence energy due to the presence of particles was insensitive to the particle relaxation time and dependent only upon the particle mass loading. They also found that the two-way coupling modified the preferential accumulation of particles. Elghobashi & Truesdell (1993) performed a DNS of particle-laden decaying homogenous turbulence. They investigated the effects of particle relaxation time, diameter, volume fraction and gravity, and showed that the presence of particles increased the fluid turbulence energy at high wavenumbers. McLaughlin (1994) suggested that since the particles considered by Elghobashi and Truesdell were smaller than the Kolmogorov length scale, they imparted their energy to the smallest eddies and as a result, they increased the energy in the highest wavenumbers. Yarin & Hetsroni (1994) studied the particle–turbulence interaction and found that finer particles damp the turbulence while coarser particles enhance it. They suggested that the level of turbulence modulation is affected by four parameters: the particle mass loading, the particle–fluid density ratio, the particle Reynolds number and the ratio of the particle diameter to a characteristic eddy diameter.

Kulick, Fessler & Eaton (1994) experimentally studied turbulence modulation in a fully developed channel flow with particles that were smaller than the Kolmogorov length scale. They showed that the fluid turbulence was attenuated by the presence of the particles, and the level of attenuation increased with particle Stokes number, particle mass loading and distance from the wall. Young & Leeming (1997) proposed a theory of particle deposition in a fully developed turbulent pipe flow using a purely Eulerian approach. They showed that turbulent diffusion flux and turbophoresis were two processes dominating the particle dynamic behaviour. Caraman, Boree & Simon (2003) used two-component phase Doppler anemometry to measure particle fluctuations in a fully developed pipe flow at a low mass loading. They observed that

the radial fluctuating velocity of the particles is similar to the axial fluctuation intensity. They claimed that this trend was because of their circular geometry. Portela & Oliemans (2003) developed a code for the DNS of particle-laden turbulent flows, using an Eulerian–Lagrangian point-particle approach. When the two-way coupling was considered, they reported that the presence of particles led to large damping in the intensity of the streamwise vortices, without any significant change in their shape and size. They also showed that this damping led to a weakening of the near-wall streaky pattern and a reduction in the accumulation of particles near the wall.

While most researchers ignored particle–particle interactions in their two-way coupling simulations, Chen, Kontomaris & McLaughlin (1997*a*, 1997*b*) found that inter-particle collisions had profound effects on particle dispersion and deposition even at very low particle volume fractions. Yamamoto *et al.* (2001) studied the interaction between turbulence and solid particles in a fully developed channel flow using large eddy simulation; they also considered inter-particle collisions at high mass loadings. They showed that the shape and scale of particle concentrations calculated considering inter-particle collision are in good agreement with experimental observations of Fessler & Eaton (1994). Li *et al.* (2001) showed that particle–particle collisions greatly reduce the tendency of particles to accumulate near the wall. Hadinoto *et al.* (2005) studied turbulence modulation for a given particle mass loading for different Reynolds numbers. According to their experimental results, the fluid fluctuating velocities increase with increasing Reynolds number, while the particle fluctuating velocities decrease as the Reynolds number increases. Their experimental results, however, suggested that the ratio of the particle diameter to the characteristic eddy diameter and the particle Reynolds number is not adequate for predicting turbulence modulation in gas–solid flows. Nasr & Ahmadi (2007) studied the effect of the two-way coupling and inter-particle collisions on turbulence modulation in a downward turbulent channel flow. They showed that when particle–particle collisions were included in the simulation, the predicted streamwise mean particle velocity profile became flatter than the fluid velocity profile due to transverse mixing, and as a result, turbulence attenuation occurred. Their simulation results were in good agreement with the experimental data of Kulick *et al.* (1994).

Vreman (2007) studied turbulence characteristics of particle-laden pipe flows using an Eulerian–Lagrangian approach, including inter-particle collisions. The inclusion of wall roughness was found to be important in achieving good agreement with the experimental data. They also showed that the particle aerodynamic interactions did not affect the results. Ayala, Grabowski & Wang (2007) incorporated a Eulerian–Lagrangian direct numerical simulation approach to study turbulent collisions of hydrodynamically interacting particles. They found that due to particle hydrodynamic interactions, the particle collision rate increased for a monodispersed system and decreased for a bidispersed system.

In this study, the effects of inter-particle collisions, two-way coupling and particle aerodynamic interaction on dispersed and carrier phase fluctuations are studied using the direct numerical simulation of the Navier–Stokes equation via a pseudo-spectral method. The particle deposition velocity, particle fluctuating velocities, particle normal velocity and particle concentration profiles were evaluated under different conditions. The cases of the one-way coupling, the two-way coupling, the four-way coupling and inter-particle collisions without two-way coupling were analysed. The effects of particle–particle collisions as well as the two-way coupling on the simulation results are discussed. The effect of aerodynamic particle interactions in addition to the four-way coupling (six-way coupling) is also examined.

2. Governing equations

2.1. *Particle phase*

The Lagrangian equation of motion of spherical particles moving in a wall-bounded channel flow, including the wall-corrected nonlinear drag and lift forces in wall units, is given as

$$\frac{\mathrm{d}\boldsymbol{u}^{+p}}{\mathrm{d}t^{+}} = C_D \boldsymbol{F}_d^{+} + \boldsymbol{F}_l^{+} \tag{1}$$

and

$$\frac{\mathrm{d}\boldsymbol{x}^{+}}{\mathrm{d}t^{+}} = \boldsymbol{u}^{+p}, \tag{2}$$

where

$$\boldsymbol{x}^{+} = \frac{\boldsymbol{x}u^{*}}{\nu} \quad t^{+} = \frac{tu^{*2}}{\nu} \quad \boldsymbol{u}^{+} = \frac{\boldsymbol{u}}{u^{*}} \tag{3}$$

Here, $\boldsymbol{u}^{+p}$ is the non-dimensional particle velocity, $\boldsymbol{u}^{+f}$ is the non-dimensional instantaneous fluid velocity at the particle location, C_D is the nonlinear drag correction factor, $\boldsymbol{F}_d^{+}$ is the drag force after including the wall drag corrections and $\boldsymbol{F}_l^{+}$ is the wall-induced and shear-induced lift force. In (3), $\boldsymbol{u}^{*}$ is the flow shear velocity.

The details of the lift force including the near-wall effects were described in the work of Chen & McLaughlin (1995) and Zhang & Ahmadi (2000) and therefore are not repeated here. (Note that only the y-component of lift force is considered in this study.)

Based on a synthesis of available experimental results, Clift, Grace & Weber (1978) and Beard & Pruppacher (1971) recommended the following nonlinear drag correction factors:

$$C_D = \begin{cases} 1.0 + 0.1875Re_p & Re_p \leqslant 0.01 \\ 1.0 + 0.1315Re_p^{0.82-0.0217\ln(Re_p)} & 0.01 \leqslant Re_p \leqslant 20 \end{cases}. \tag{4}$$

Here, $Re_p = d^{+}|\boldsymbol{u}^{+f} - \boldsymbol{u}^{+p}|$ is the particle Reynolds number. Additional details of the drag and lift forces were described in detail by Chen & McLaughlin (1995) and Ounis *et al.* (1991).

The non-dimensional particle relaxation time is defined as

$$\tau^{+} = S\frac{d^{+^2}}{18}, \tag{5}$$

where $d^{+} = \mathrm{d}u^{*}/\nu$ is the non-dimensional particle diameter and S is the particle-to-fluid density ratio.

For evaluating the forces acting on the particles, the fluid velocities at the locations of particles must be evaluated using an interpolation technique. An accurate evaluation of particle velocities is also essential for analysis of inter-particle collisions that depend on the often small relative particle velocities. In this study, partial Hermite interpolation method was used for evaluating the fluid velocities at the locations of particles and for the inverse action of particle drag on the fluid.

To evaluate the particle deposition velocity, it is assumed that when a particle reaches a distance of one radius from the wall, it deposits with no rebound. In order to keep a uniform particle concentration inside the channel, when a particle is deposited on the wall, another particle is randomly introduced in the computational domain.

The hard sphere particle–particle collision model with a coefficient of restitution equal to 0.95 was used in the analysis. The procedure for the numerical implementation of the particle–particle collisions as described by Li *et al.* (2001) was implemented in the present analysis. In this study, the collisions were assumed to be binary since multiple collisions are extremely rare at the particle concentrations that were considered.

3. Particle aerodynamic interactions

In addition to the interaction of particles with the gas, the motion of each particle may be affected by the presence of other nearby particles in the flow. As a result, the particle aerodynamic interaction could influence the particle collision rate, as well as the particle and fluid phase fluctuations. Ardekani & Rangel (2006) employed the method of reflections combined with Burger's unsteady flow solution to study the unsteady motion of two spherical solid particles in an unbounded incompressible Newtonian flow. In their study, the interacting particles were sufficiently far from the walls so that the surrounding fluid could be regarded as infinite. The advantage of this method is that it can be extended to a large number of particles, and the background flow can be time dependent. The drawback of this method is that the solution loses its inaccuracy as the particles get very close to each other.

Based on the work of Ardekani & Rangel (2006), Vreman (2007) studied the effect of particle aerodynamic interaction in two-phase flows. Accordingly, particle velocity (particle a) must be corrected by the effect of all nearby particles (particle b) before computing the drag force. That is

$$\left(\boldsymbol{u}^{+p^a}\right) = \boldsymbol{u}^{+p^a} + \sum_{b=1}^{N}\left[\frac{c_1^2}{1-c_1^2}\left(\boldsymbol{u}^{+p^a}-\boldsymbol{u}^{+f^a}\right)_n - \frac{c_1}{1-c_1^2}\left(\boldsymbol{u}^{+p^b}-\boldsymbol{u}^{+f^b}\right)_n + \frac{c_2^2}{1-c_2^2}\left(\boldsymbol{u}^{+p^a}-\boldsymbol{u}^{+f^a}\right)_t - \frac{c_2}{1-c_2^2}\left(\boldsymbol{u}^{+p^b}-\boldsymbol{u}^{+f^b}\right)_t\right]. \quad (6)$$

Here, the superscript b corresponds to particle b (which is one of the particles near particle a) and N is the number of neighbouring particles taken into consideration. The vector $\hat{\boldsymbol{n}}$ is a unit vector pointing from particle a to particle b. In (6), the normal and tangential relative velocities are defined as

$$(\boldsymbol{u}^{+p}-\boldsymbol{u}^{+f})_n = ((\boldsymbol{u}^{+p}-\boldsymbol{u}^{+f})\cdot\hat{\boldsymbol{n}})\,\hat{\boldsymbol{n}} \quad (\boldsymbol{u}^{+p}-\boldsymbol{u}^{+f})_t = \boldsymbol{u}^{+p}-\boldsymbol{u}^{+f}-(\boldsymbol{u}^{+p}-\boldsymbol{u}^{+f})_n. \quad (7)$$

The coefficients in (6) are given as

$$c_1 = \frac{3}{4}\varepsilon + \frac{1}{2}\varepsilon^3, \quad c_2 = \frac{3}{2}\varepsilon - \varepsilon^3, \quad \varepsilon = \frac{d^+}{2\,|\boldsymbol{r}^+|}, \quad (8)$$

where $\boldsymbol{r}^+$ is the distance vector from particle a to particle b.

As expected, the effect of neighbouring particles on particle a decays with distance. In the computation, typically N nearest neighbouring particles within a distance of $30 \times d^+$ from particle a are taken into account. Ayala *et al.* (2007) showed that the simulation results were insensitive to the inclusion of particles at distances greater than $30 \times d^+$.

4. Gas phase

The instantaneous fluid velocity field in the channel is evaluated by DNS of the Navier–Stokes equation using an additional source term due to the presence of particles. It is assumed that the flow is incompressible, and a constant mean pressure gradient in x-direction is imposed. The corresponding governing equations of motion are as follows.

Continuity equation. In this study, the volume fraction of particles is very small, $\phi_v < 10^{-3}$; therefore, the continuity equation may be expressed as

$$\nabla \cdot \boldsymbol{u}^{+f} = 0. \tag{9}$$

Momentum equation. The effect of particles is added to the Navier–Stokes equations by an additional source term using the point force model:

$$\frac{D\boldsymbol{u}^{+f}}{Dt^+} = -\nabla^+ p^+ - \frac{1}{H^+}\hat{i} + \nabla^{+2}\boldsymbol{u}^+ + S_{\boldsymbol{u}}^{p+}, \tag{10}$$

where $\boldsymbol{u}^{f+} = (u^{f+}, v^{f+}, w^{f+})$ is the fluid velocity vector in wall units, and p^+ is the pressure in wall units. The coupling between fluid and dispersed phases was incorporated into the momentum equation via a feedback force per unit mass, which is the negative of the drag and lift forces acting on the particles exerted by the fluid in a certain computational cell; the particle feedback force per unit mass is given by

$$S_{\boldsymbol{u}}^{p+} = -\sum_{n=1}^{N^P} \frac{\mathrm{d}\boldsymbol{u}^{p+}}{\mathrm{d}t^+} = -\sum_{n=1}^{N^P} (C_D \boldsymbol{F}_d^+ + \boldsymbol{F}_l^+). \tag{11}$$

No-slip boundary conditions are assumed on the channel walls and periodic boundary conditions are imposed in the x- and z-directions as follows:

$$\left.\begin{aligned} &\boldsymbol{u}^{f+} = 0, \quad y^+ = \pm H^+, \\ &\boldsymbol{u}^{f+}(x^+ + m\lambda_x^+, y^+, z^+ + n\lambda_z^+, t^+) = \boldsymbol{u}^{f+}(x^+, y^+, z^+, t^+), \end{aligned}\right\} \tag{12}$$

where m and n are integers.

In the present simulations, a channel that has half-width H^+ in wall units and a $\lambda_x^+ \times \lambda_z^+$ periodic segment in x- and z-directions is used. A schematic of the flow domain and the periodic cell are shown in figure 1. An $nx \times ny \times nz$ computational grid in the x-, y- and z-directions is employed. The grid spacing in the x- and z-directions is constant, while the variation of grid points in the y-direction is determined by the collocation points of the Chebyshev series. The distance of the ith grid point in the y-direction from the centreline is given as

$$y_i^+ = \frac{H^+}{2}\cos(\pi i/M), \quad 0 \leqslant i \leqslant M, \tag{13}$$

where $M = nz - 1$.

The channel flow code used in this study is the one developed by McLaughlin (1989). The code used a pseudo-spectral method for computing the fluid velocity field. That is, the fluid velocity is expanded in a three-dimensional Fourier–Chebyshev series. The fluid velocity field is expanded in Fourier series in the x- and z-directions, while in the y-direction a Chebyshev series is used. The code uses an Adams–Bashforth–Crank–Nickolson (ABCN) scheme to compute the nonlinear and viscous terms in the Navier–Stokes equation and performs three fractional time steps to advance the fluid velocity from time step (n) to time step $(n+1)$. The details of the numerical techniques were described by McLaughlin (1989).

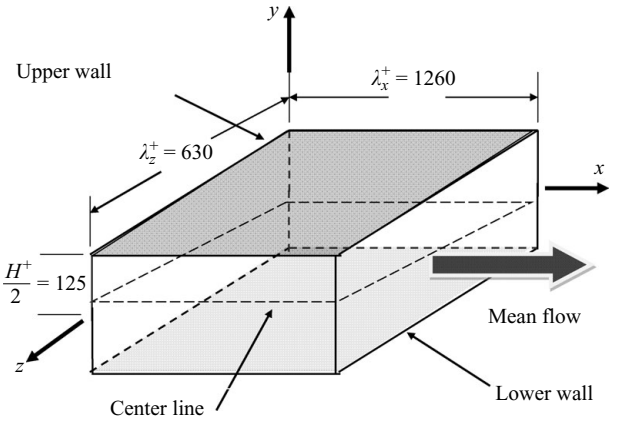

FIGURE 1. Schematics of the channel flow and the computational periodic cell used.

Typically, a temperature of 288 K, $\nu = 1.5 \times 10^{-5}\,\mathrm{N\,s\,m^{-2}}$ and $\rho^f = 1.2\ \mathrm{kg\ m^{-3}}$ for air were used. The friction velocity, $\boldsymbol{u}^*$, was assumed to be $0.3\,\mathrm{m\,s^{-1}}$. The channel half-width was $H^+ = 125$ and the streamwise and spanwise periods were, respectively, $\lambda_x^+ = 1260$ and $\lambda_z^+ = 630$. The numbers of grid points in the x-, y- and z-directions were $nx = 64$, $ny = 65$ and $nz = 64$, respectively. Simulations were also performed in a smaller region (with $\lambda_x^+ = 630$) and the results did not show any noticeable difference. The Reynolds number based on the friction velocity, $\boldsymbol{u}^*$, and the half channel width was 125, while the flow Reynolds number based on the hydraulic diameter and the centreline velocity was about 8000. This condition corresponds to a channel half-width, $H = 12.5\,\mathrm{mm}$, and streamwise and spanwise periods equal to 31.5 mm. The value for the density ratio, $S = \rho^p/\rho^f$, was taken to be 1000. To focus on gas–solid interactions, the effect of gravity was neglected.

Each simulation was performed for 5000 time steps, and the non-dimensional time step was chosen to be 0.25 in wall units. Thus, the period of a simulation was 1250 wall units. The interval from 250 to 1250 wall units was used for evaluating various statistics. Simulations were performed for particle diameters of $d = 25$ and $30\,\mu\mathrm{m}$; the corresponding values of the non-dimensional particle relaxation time are, respectively, $\tau^+ = 14$ and 20. It should be emphasized that the period of the simulations is much larger than that of the non-dimensional particle relaxation time. Therefore, a statistically quasi-steady state is achieved and the effect of initial conditions of particles is eliminated.

Simulations were performed at particle mass loadings of ML = 20 % and 40 %. Note that for particles with $\tau^+ = 14$ and ML = 40 %, approximately 12 00 000 particles were tracked. All results have been averaged over the simulation time, and over the streamwise and spanwise directions. Particles were uniformly distributed in the channel, and the initial velocity of each particle was set equal to the local fluid velocity evaluated at the centre of the particle.

5. Results and discussions

In this section, simulation results for different particle parameters such as particle fluctuation velocities, particle streamwise and normal velocities, particle deposition velocity and particle concentration are presented. To clarify the relative importance of various effects, all simulations were performed under different conditions and the

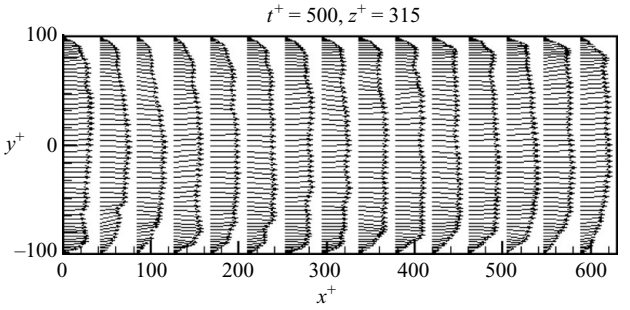

FIGURE 2. Sample velocity vector plot in the x–y plane, one-way coupling.

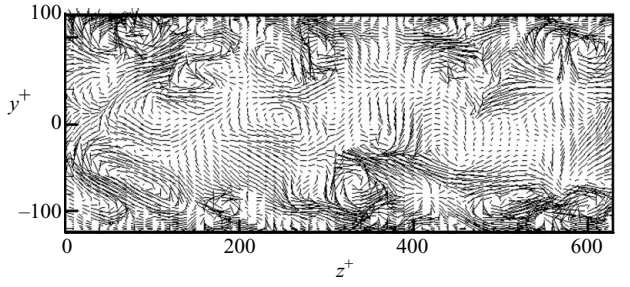

FIGURE 3. Velocity vector plot in the y–z plane in the presence of $\tau^+ = 20$ particles, the one-way coupling.

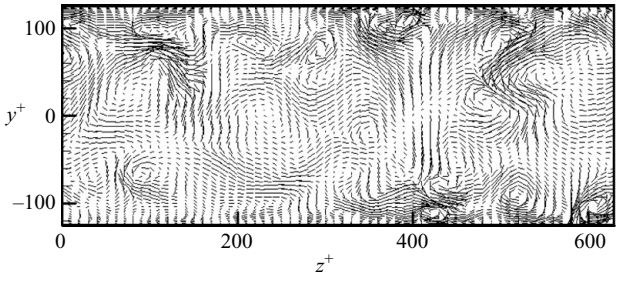

FIGURE 4. Velocity vector plot in the y–z plane in the presence of $\tau^+ = 20$ particles, the four-way coupling at ML = 20 %.

results are compared. These are: (i) the one-way coupling; (ii) the two-way coupling; (iii) the four-way coupling; and (iv) including inter-particle collisions, but neglecting the two-way coupling and particle aerodynamic interactions. Several simulations were also performed where the effect of particle aerodynamic interactions were accounted in the analysis (six-way coupling). A comparison of the results for different cases is used to assess the relative contributions of the two-way coupling, inter-particle collisions, as well as the six-way coupling on various particle velocity statistics.

Figure 2 shows a sample instantaneous velocity vector plot in the x–y plane at $t^+ = 500$ in the case of the one-way coupling. The random deviations from the expected mean velocity are clearly seen in this figure. Figures 3–5 show the velocity field in the y–z plane at $t^+ = 500$ in the cases of the one-way and four-way couplings at mass loadings of ML = 20 % and ML = 40 %, respectively. The near-wall coherent

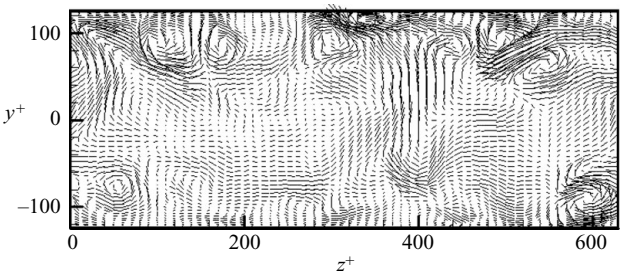

FIGURE 5. Velocity vector plot in the y–z plane in the presence of $\tau^+ = 20$ particles, the four-way coupling at ML = 40 %.

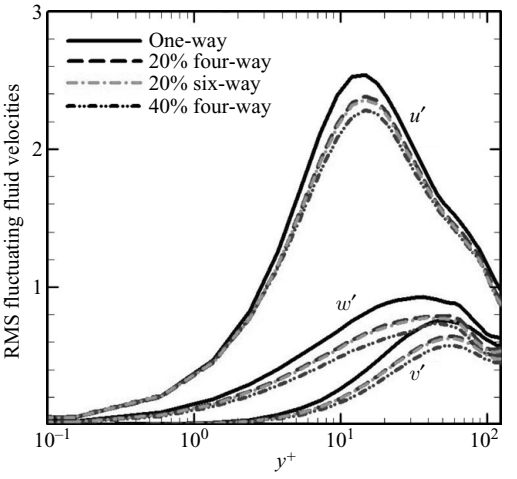

FIGURE 6. Effects of $\tau^+ = 20$ particles on the flow fluctuating velocities.

eddies and flow streams towards and away from the wall can be observed in these figures. Comparing the results of the one-way coupling in figure 3 with those of the four-way coupling in figures 4 and 5, it appears that the presence of solid particles damps the turbulence fluctuations and also decreases the number of eddies. These observations are in agreement with the experimental results of Rashidi *et al.* (1990). It is also seen that as particle mass loading increases, the level of damping increases.

The simulated root-mean square (RMS) fluctuation fluid velocities in the cases of the one-way, four-way and six-way couplings at mass loadings of 20 % and 40 % are shown in figure 6. It is seen that the addition of particles with $\tau^+ = 20$ attenuates the intensity of the fluctuations, and as particle mass loading increases, the level of attenuation increases. This trend is in agreement with earlier experimental data and numerical results. As noted earlier, particles with diameter less than the Kolomogorov length scale attenuate the turbulence, while particles with diameters larger than the Kolmogorov length scale augment it. Moreover, the inclusion of particle aerodynamic interactions has no significant effects on the flow fluctuating velocities compared with the four-way coupling case.

Figure 7 shows the variation of the Kolmogorov length scale, evaluated from the average dissipation rate, versus the distance from the wall. The Kolmogorov scale varies from $\eta = 85\,\mu$m at the wall to $\eta = 160\,\mu$m at the channel centreline. The largest

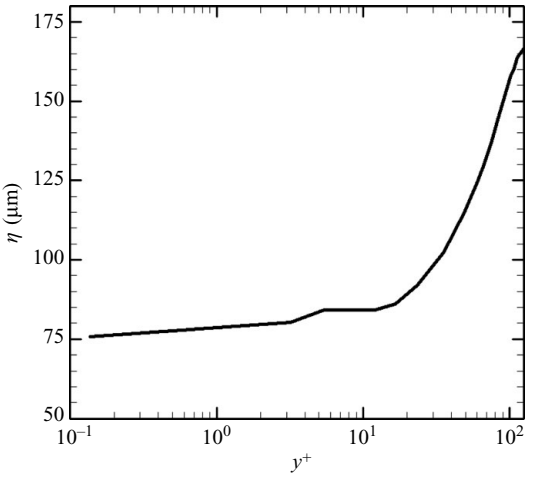

FIGURE 7. Kolmogorov length vs. the distance from the wall.

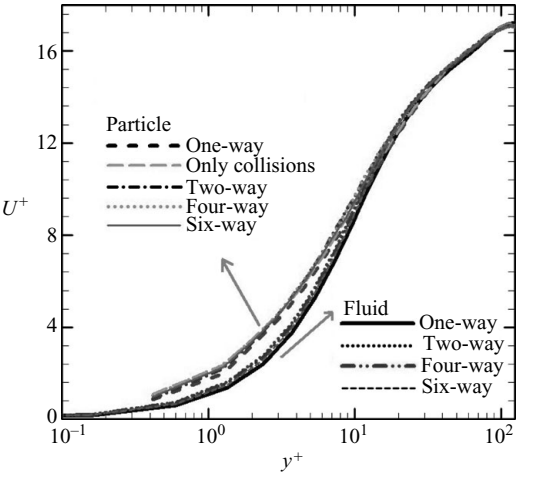

FIGURE 8. Mean streamwise particle velocity vs. the distance from the wall for $\tau^+ = 20$ particles at ML = 20 %.

particle diameter tracked in this study is 30 μm, which is smaller than the Kolmogorov length scale.

Figure 8 shows the fluid and particle streamwise velocity versus the distance from the wall for $\tau^+ = 20$ particles at ML = 20 %. It is observed that the two-way coupling, inter-particle collisions and particle aerodynamic interactions have no significant effect on the fluid and particle streamwise velocity profiles. It should be emphasized that here a constant pressure drop is imposed and the gravity is neglected.

Figures 9 and 10, respectively, show the average particle Reynolds number (Re_p) versus the distance from the wall for particles with τ^+ of 20 and 14 for different cases. The particle Reynolds number is defined based on the particle diameter and the particle slip velocity relative to the fluid. That is, $Re_p = d^+|\boldsymbol{u}^{+p} - \boldsymbol{u}^{+f}|$. It is observed that the maximum value for particle Reynolds number occurs in the wall region due to the relatively large values of slip velocity, $|\boldsymbol{u}^{+p} - \boldsymbol{u}^{+f}|$. For the two-way coupling case, figure 9 shows that the particle Reynolds number decreases compared with the

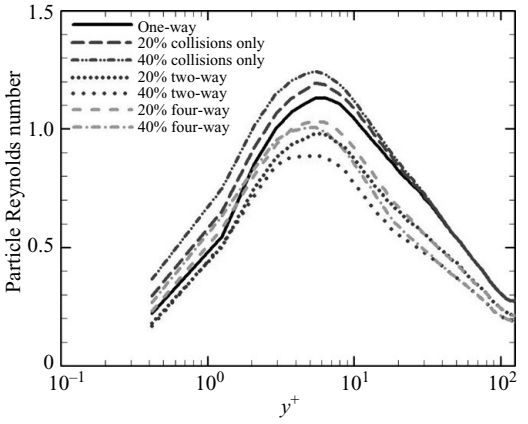

FIGURE 9. Particle Reynolds number vs. the distance from the wall for particles with $\tau^+ = 20$.

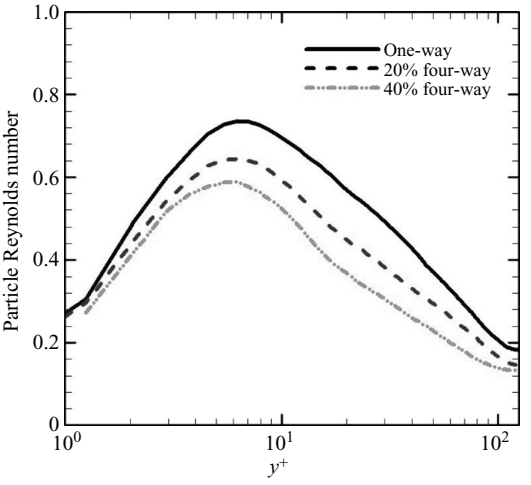

FIGURE 10. Particle Reynolds number vs. the distance from the wall for particles with $\tau^+ = 14$.

one-way coupling condition. In contrast, the inter-particle collisions increase the particle Reynolds number. For the four-way coupling case, the Reynolds number decreases in the core region; however, the amount of decrease is less than the decrease observed under the two-way coupling conditions. In the wall region, the particle Reynolds number is slightly larger than that of the one way-coupling case. In summary, inter-particle collisions increase the particle Reynolds number, while the two-way coupling decreases it. When both collisions and the two-way coupling are present (i.e. the physical situation), the particle Reynolds number decreases somewhat in the core region and increases in the wall region. Figure 10 further shows that as the mass loading increases, the particle Reynolds number decreases.

Figures 9 and 10 imply that the nonlinear drag correction needs to be included in the analysis. The peak particle Reynolds number appears to be of the order of unity; hence, the nonlinear drag coefficient is nearly 15 % larger than the Stokes drag.

Figures 11 and 12, respectively, show the number of deposited particles versus time for relaxation times, τ^+, of 14 and 20 for different cases. Since in each case the

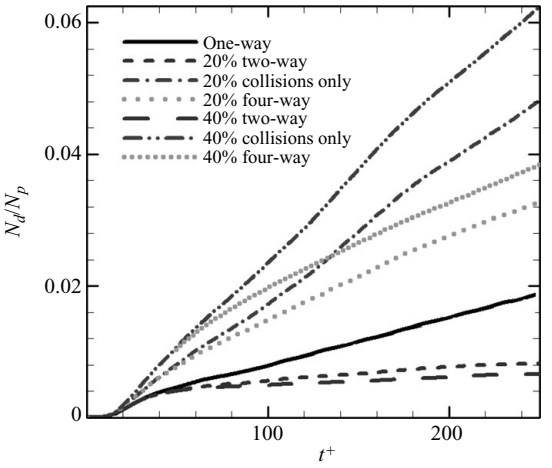

FIGURE 11. Normalized number of deposited particles vs. non-dimensional time for particles with $\tau^+ = 14$.

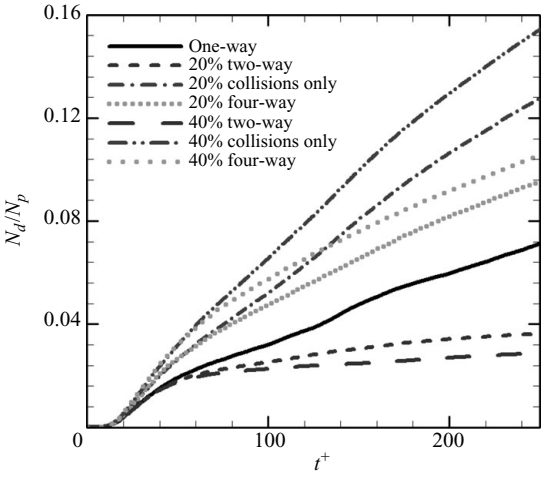

FIGURE 12. Normalized number of deposited particles vs. non-dimensional time for particles with $\tau^+ = 20$.

number of particles is different; the number of deposited particles in this figure is normalized by the total number of particles being tracked. In the case of the two-way coupling (neglecting collisions), the number of deposited particles decreases as the particle mass loading increases. In the case of the four-way coupling, in which both the particle feedback force and inter-particle collisions are present, the number of deposited particles increases as the particle mass loading increases. When the effect of particles on the flow is neglected but the inter-particle collisions are taken into account, the number of deposited particles increases even faster as particle mass loading increases. In summary, for the range of parameters studied, the simulation results suggest that the two-way coupling causes a decrease in the number of deposited particles, while inter-particle collisions lead to an increase in the number of deposited particles. The increase in the number of deposited particles due to inter-particle

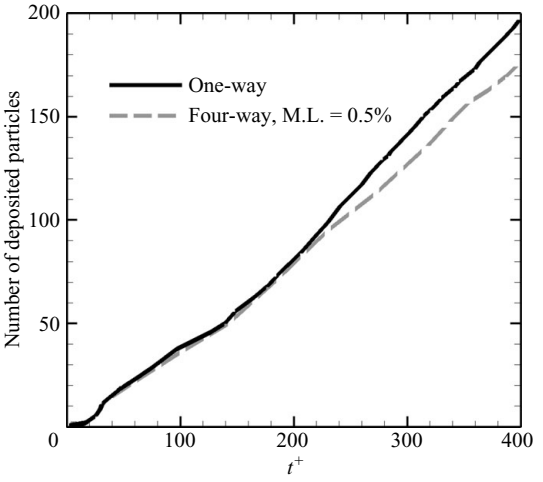

FIGURE 13. Number of deposited particles vs. non-dimensional time for particles with $\tau^+ = 20$ at ML = 0.5 %.

collisions is larger than the decrease caused by the two-way coupling effects. Thus, for the four-way coupling case, the number of deposited particles increases with mass loading.

It is also of interest to provide insight into the importance of the two-way coupling as well as the inter-particle collisions on the particle deposition rate at low particle mass loadings. For this purpose, computer simulations were performed for $\tau^+ = 20$ particles at the low mass loading of 0.5 % under the four-way coupling conditions and the results are plotted in figure 13. It is observed that the number of deposited particles decreases compared with the one-way coupling case. This implies that at very low particle mass loadings, the damping effect of the two-way coupling on the particle deposition rate is more effective than the enhancement induced by the inter-particle collisions effect. In fact, the two-way coupling effect is roughly linear in particle mass loading, while the collisional effects are expected to exhibit quadratic dependence on the mass loading (since it involves binary collisions). As a result, at very low particle mass loadings, the two-way coupling effects dominant the particle collision effects.

Comparing figures 11 and 12, it may be seen that the number of deposited particles increases as relaxation time increases. This observation is in agreement with the earlier simulation results of McLaughlin (1989), Chen & McLaughlin (1995) and Ounis *et al.* (1991). The simulations were also repeated for $\tau^+ = 35$ and 50 and the results show similar trends. These simulation results are not shown here due to space limitations.

6. Particle deposition velocity

In the aerosol community, deposition velocity is used as a convenient parameter for presenting the deposition rate data. For a uniform particle concentration, C_0, the non-dimensional deposition velocity is defined as

$$u_d^+ = J/C_0 u^*, \tag{14}$$

where J is the particle mass flux to the wall per unit time. In the computer simulation, the particle deposition velocity on one wall may be estimated as (Zhang & Ahmadi 2000)

$$u_d^+ = \frac{(N_d)/t_d^+}{(N_p)/(H^+)}, \tag{15}$$

where N_p is the total number of the particles in the channel, and N_d is the number of deposited particles that deposit on the channel walls in the time interval t_d^+.

A simple empirical equation for the non-dimensional deposition velocity in duct flows is suggested by Wood (1981). That is

$$u_d^+ = 0.084\, Sc^{-2/3} + 4.5 \times 10^{-4} \tau^{+^2}, \tag{16}$$

where $Sc = \nu/D$ is the Schmidt number with D being the particle mass diffusivity given as

$$D = \frac{kT}{3\pi\mu d} C_c, \tag{17}$$

The first term in (16) is particle deposition due to Brownian motion as derived by Cleaver & Yates (1975), and the second term is particle deposition due to the so-called eddy diffusion–impaction.

Fan & Ahmadi (1993) developed a more detailed empirical equation for the deposition of particles in vertical ducts including the effects of surface roughness, lift force and gravity along the flow direction. That is

$$u_d^+ = \begin{cases} 0.084 Sc^{-2/3} + \dfrac{1}{2}\left[\dfrac{\left(0.64k^+ + \dfrac{1}{2}d^+\right)^2 + \dfrac{\tau^{+^2} g^+ L_1^+}{0.01085(1+\tau^{+^2}L_1^+)}}{3.42 + (\tau^{+^2} g^+ L_1^+)/(0.01085(1+\tau^{+^2}L_1^+))}\right]^{1/(1+\tau^{+^2}L_1^+)} \\ \quad \times \left[1 + 8\mathrm{e}^{-(\tau^+ - 10)^2/32}\right] \dfrac{0.037}{1 - \tau^{+^2} L_1^+ (1 + (g^+/0.037))} & \text{if} \quad u_d^+ < 0.14 \\ 0.14 & \text{otherwise.} \end{cases} \tag{18}$$

Here $L_1^+ = 3.08/(Sd^+)$, $g^+ = (\nu/u^{*3})g$ and k^+ is the surface roughness which is equal to zero for smooth surfaces.

Figure 14 shows the simulated non-dimensional deposition velocity, $\boldsymbol{u}_d^+$, versus the non-dimensional particle relaxation time, τ^+ for different cases. In this figure , the experimental data of Papavergos & Hedley (1984), the empirical equation of Wood (1981), the simulation results of Li & Ahmadi (1992), McLaughlin (1989), He & Ahmadi (1999) and Zhang & Ahmadi (2000), and the empirical model prediction of Fan & Ahmadi (1993) for dilute suspensions are shown for comparison. The collected experimental data reported by Papavergos & Hedley (1984) have a considerable scatter. As noted by Fan & Ahmadi (1993) and Zhang & Ahmadi (2000), this is in part due to variations in shear velocity, density ratio and the direction of flow. The statistical error for the simulation based on the number of deposited particle is of the order of 0.5%–1 %. The present simulation results for the one-way coupling case are in favourable agreement with the experimental data and earlier simulation results. It is observed that as the particle relaxation time increases, the particle deposition velocity also increases.

Figure 14 also shows that the deposition velocity varies with the mass loading. In the case of the four-way coupling both damping effects of particles and particle collisional

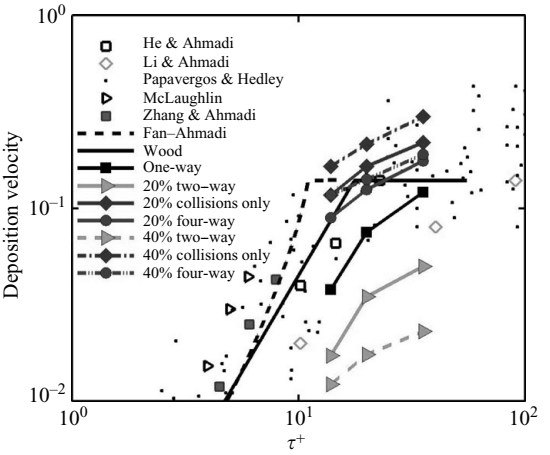

FIGURE 14. Non-dimensional particle deposition velocity vs. non-dimensional particle relaxation time.

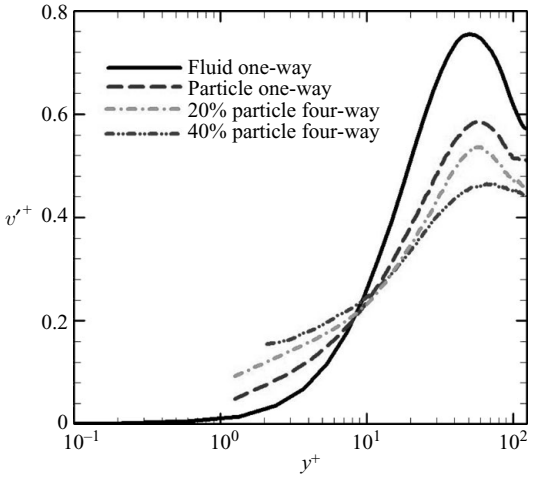

FIGURE 15. Normal fluctuating velocity vs. the distance from the wall for particles with $\tau^+ = 14$.

effects are included (the four-way coupling), the particle deposition velocity increases as the mass loading increases. When the particle collision effects are neglected in the simulations, the two-way coupling effects cause a decrease in the particle deposition velocity as turbulence is damped by the increase of particle mass loading. This figure also shows that the inter-particle collisions increase $\boldsymbol{u}_d^+$ as mass loading increases. Note that particles with equal relaxation times, τ^+, may have different diameters and density ratios; this implies that particles with equal relaxation times behave differently when inter-particle collisions are included in the simulations.

For particle deposition, the normal component of particle fluctuating velocity plays a crucial role. Figures 15–17 show the RMS normal fluctuating velocity of the airflow and particles with $\tau^+ = 14$ and 20 for different cases. In figure 15, only the one- and four-way coupling results are shown, while in figures 16 and 17 the limiting cases of the two-way coupling with no collision and only collisions are also shown for comparison. Several features in these figures are noteworthy. The normal fluctuating

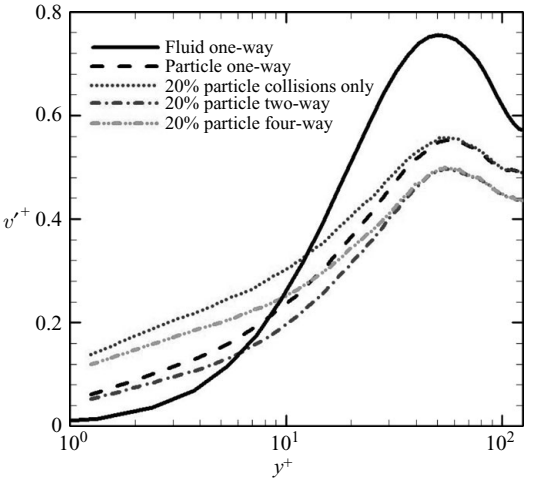

FIGURE 16. Normal fluctuating velocity vs. the distance from the wall for particles with $\tau^+ = 20$ at ML = 20 %.

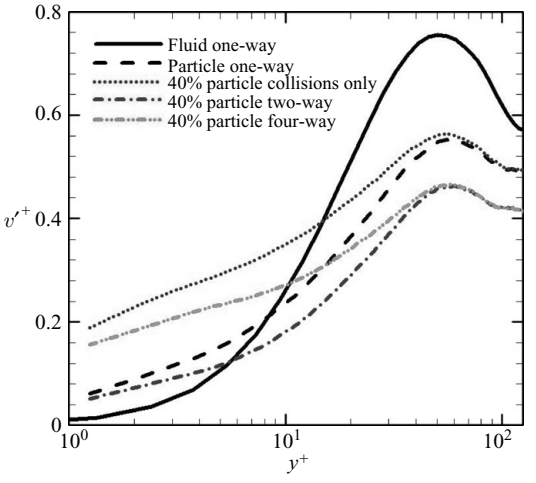

FIGURE 17. Normal fluctuating velocity vs. the distance from the wall for particles with $\tau^+ = 20$ at ML = 40 %.

velocity of particles in the case of the one-way coupling is less than the fluid in the $y^+ > 10$ region and is greater than the fluid in the wall region ($y^+ < 10$). The decrease of the fluctuating velocity of the particles in the outer region is due to the fact that the inertial particles are not fully responsive to all turbulent eddies, and they fluctuate less than the flow. The increase of the normal fluctuating velocity of the particles in the wall region is perhaps due to the fact that, as a particle migrates towards the wall, it tends to retain the velocity it possessed when it was farther from the wall. Therefore, a wide range of particle velocities are found in the wall region, causing an increase in the normal particle fluctuating velocity.

Figures 16 and 17 show that, for the case of the two-way coupling (in the absence of collision), the particle normal fluctuating velocity is lower in the entire channel in comparison to the one-way coupling case, and also decreases as particle mass loading increases. This trend can be explained in terms of turbulence attenuation effects due

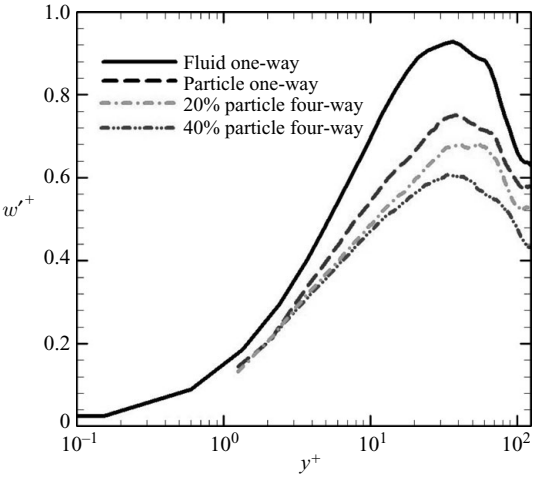

FIGURE 18. Spanwise fluctuating velocity vs. the distance from the wall for particles with $\tau^+ = 14$.

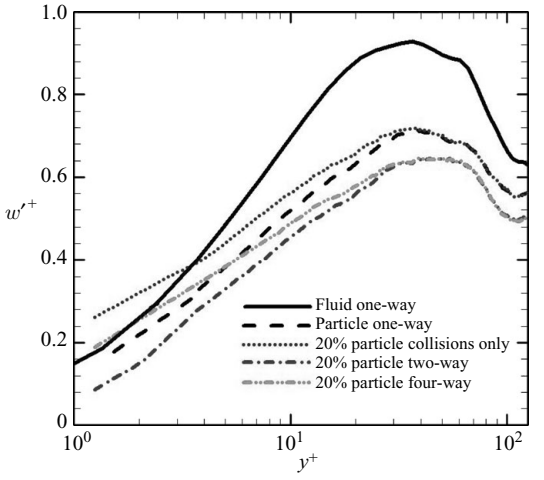

FIGURE 19. Spanwise fluctuating velocity vs. the distance from the wall for particles with $\tau^+ = 20$ at ML = 20 %.

to the presence of the particle feedback force as discussed before. When the particle feedback force is ignored but inter-particle collisions are included in the simulation, the particle normal fluctuating velocity increases in the entire channel compared with one-way coupling simulation, and as particle mass loading increases, the level of augmentation in particle normal fluctuating velocity increases. In the case of the four-way coupling, the particle normal fluctuating velocity decreases in the outer region with $y^+ > 10$ and increases in the wall region with $y^+ < 10$ compared with the one-way coupling case. These results indicate that the two-way coupling effects decrease the particle normal fluctuating velocity, while inter-particle collisions enhance it.

It is also of interest to study the effects of inter-particle collisions and the two-way coupling on the particle spanwise and streamwise fluctuating velocities. Figures 18–20 show the RMS spanwise fluctuating velocity of the airflow and particles with $\tau^+ = 14$ and 20 for different cases. It is observed that in the case of the one-way coupling

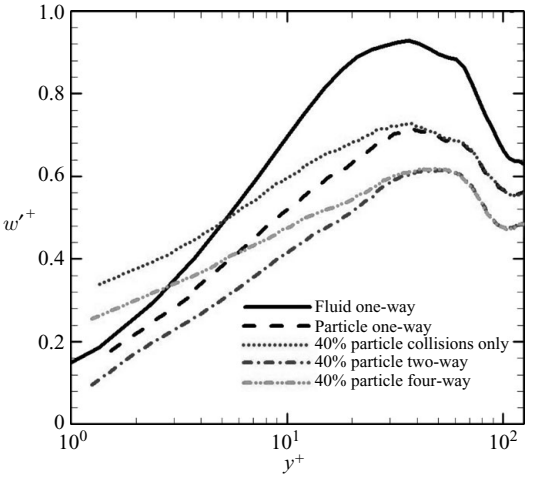

FIGURE 20. Spanwise fluctuating velocity vs. the distance from the wall for particles with $\tau^+ = 20$ at ML = 40 %.

the particle spanwise fluctuating velocity is less than that of the fluid in the entire channel. As noted before, this is because the inertial particles do not respond to all turbulence eddies. The simulation results for the two-way coupling case (in the absence of collisions) show that the particle spanwise fluctuating velocity decreases compared with the one-way coupling case as the particle mass loading increases. This trend is consistent with the turbulence attenuation due to the presence of small particles. In contrast, when the damping effects of particles through the feedback on the flow are ignored but inter-particle collisions are included in the simulation, the particle spanwise fluctuating velocity increases in the entire channel compared to the one-way coupling as mass loading increases. In the physical case of the four-way coupling that includes both damping and collision effects, the particle spanwise fluctuating velocity decreases in the region with $y^+ > 4$ and increases very close to the wall with $y^+ < 4$ compared with the one-way coupling case.

One may ask why the particle normal fluctuating velocity near the wall increases compared with the fluid one, while the particle spanwise fluctuating velocity is less than the flow one near the wall. This is because there is a particle flux towards the walls, with the maximum flux occurring in the wall region. Therefore, a wide variety of particle normal velocities exist near the wall, and this causes an increase in the RMS particle normal velocity near the wall. Since there is no mean velocity gradient in the spanwise direction, the migration of particles towards the wall does not alter the statistics of the particle spanwise velocity fluctuations.

Unlike v'^p and w'^p, it is observed in figures 21–23 that the particle streamwise fluctuating velocity exceeds the fluid streamwise fluctuating velocity. This is due to the migration of particles from the channel core towards the wall region. Since particles with $\tau^+ = 14$ and 20 tend to retain their velocities, this leads to a wide range of particle streamwise velocities in the wall region. As a result, the particle streamwise mean and fluctuating velocity increase. In the case of the two-way coupling, the particle streamwise fluctuating velocity decreases compared with the one-way coupling case due to the damping of turbulence. As particle mass loading increases, the level of attenuation in the particle streamwise fluctuating velocity increases. Furthermore, inter-particle collisions (in the absence of the two-way coupling) slightly increase the

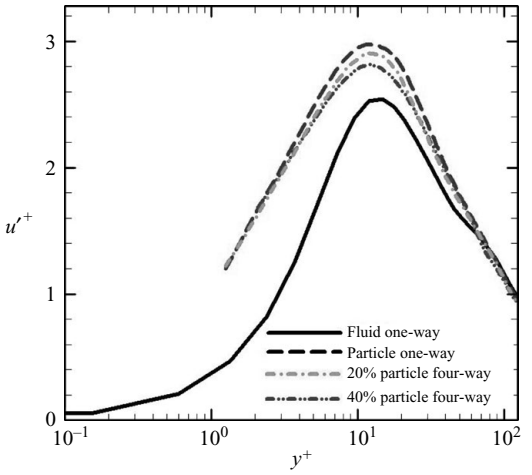

FIGURE 21. Streamwise fluctuating velocity vs. the distance from the wall for particles with $\tau^+ = 14$.

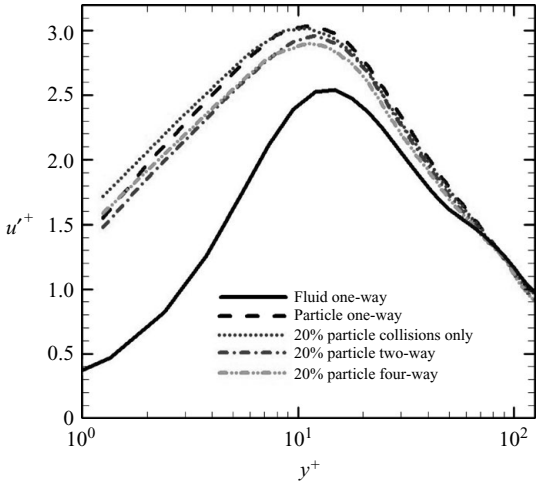

FIGURE 22. Streamwise fluctuating velocity vs. the distance from the wall for particles with $\tau^+ = 20$ at ML = 20 %.

particle streamwise fluctuating velocity near the wall, but have no noticeable effect in the channel core region. In the case of the four-way coupling, the particle streamwise fluctuating velocity decreases in comparison with the one-way coupling case. Also, as particle mass loading increases, the particle streamwise fluctuating velocity decreases. This is mainly due to the damping effect of the two-way coupling.

To assess the importance of particle aerodynamic interactions, simulations for particles with a relaxation time of $\tau^+ = 20$ at a mass loading of 20 % were performed in which the effect of aerodynamic interactions was included into the four-way coupling analysis. The results of this so-called six-way coupling model are shown in figure 24. The inclusion of particle aerodynamic interactions has no noticeable effect on the particle fluctuating velocities.

Figures 25 and 26 show, respectively, the particle mean normal velocity ($\bar{v}^{p^+}$) for $\tau^+ = 14$ and 20 for different scenarios. Despite the zero-mean normal fluid velocity,

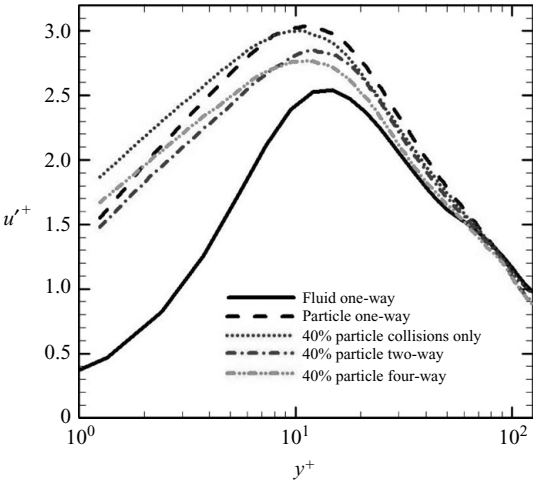

FIGURE 23. Streamwise fluctuating velocity vs. the distance from the wall for particles with $\tau^+ = 20$ at ML = 40 %.

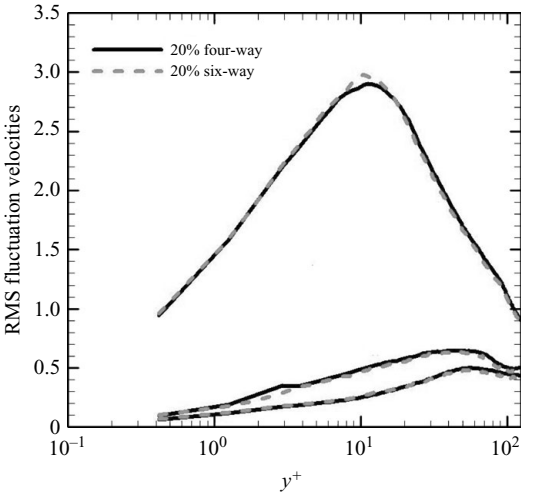

FIGURE 24. Streamwise fluctuating velocity vs. the distance from the wall for $\tau^+ = 20$ particles at ML = 20 %.

there is a particle flux towards the wall with a maximum value occurring at about $y^+ = 20$. In the case of the two-way coupling, the particle normal mean velocity decreases compared with the one-way coupling case. These figures show that inter-particle collisions decrease the mean particle normal velocities outside the viscous sublayer region with $y^+ > 5$ and increase it in the sublayer region with $y^+ < 5$. In the case of the four-way coupling, the decrease in the mean particle normal velocity is higher than the decrease in the case of the two-way coupling for $y^+ > 5$. In summary, inter-particle collisions decrease the particle mean normal velocity in the region where $y^+ > 5$ and increase it in the wall region. The two-way coupling, however, decreases the mean particle normal velocities in the entire channel.

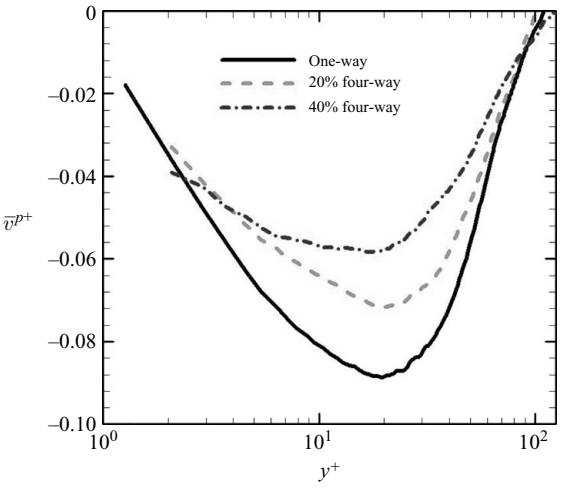

FIGURE 25. Normal particle velocity vs. distance from the wall for particles with $\tau^+ = 14$.

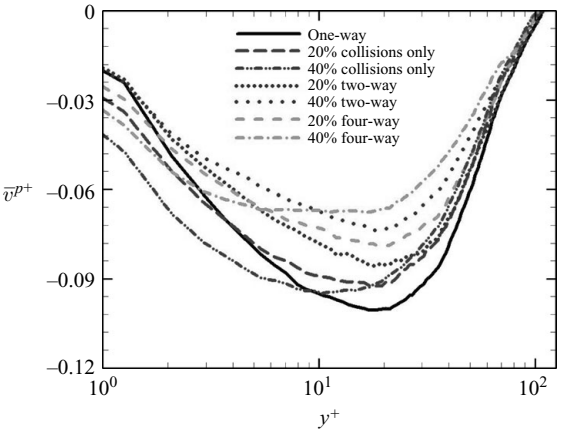

FIGURE 26. Normal particle velocity vs. distance from the wall for particles with $\tau^+ = 20$.

7. Particle concentration

In this section, the effects of the two-way coupling and inter-particle collisions on the particle concentration profiles are investigated. The particle concentration profiles versus the distance from the wall for $\tau^+ = 14$ and 20 particles at mass loadings of 20 % and 40 %, respectively, are shown in figures 27 and 28. The mean concentration profiles here are normalized by the bulk concentration. It is seen from the figures that the maximum accumulation of particles near the wall occurs in the case of the one-way coupling. In fact, it was shown by Ounis *et al.* (1993) and Chen & McLaughlin (1995) that the particle accumulation in the wall region is due to the wall coherent eddies. Both two-way coupling and inter-particle collisions reduce the concentration of particles near the wall. Therefore, in the case of the four-way coupling, in which both two-way coupling and inter-particle collisions are present, one finds the minimum particle accumulation near the wall. Increasing particle mass loading intensifies the effects leading to a larger decrease in particle accumulation near the wall. In the case of the one-way coupling, the near-wall eddies strongly interact with suspended

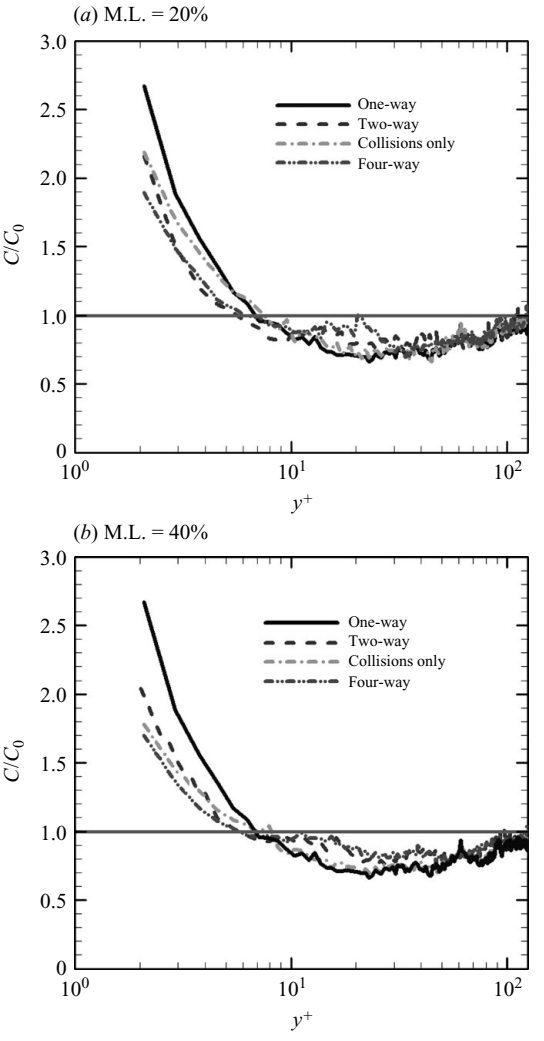

FIGURE 27. Particle concentration profile for different cases, $\tau^+ = 14$, (*a*) ML = 20 % (*b*) ML = 40 %.

particles. Inter-particle collisions randomize the particle trajectories and reduce the effect of near-wall eddies on the particles, and two-way coupling damps the turbulent eddies. As a result, the particle concentration near the wall decreases.

Figures 25 and 26 show that there is a small drift of particles towards the wall, and the magnitude of the drift decreases with mass loading. Figures 15–17 show that the near-wall fluctuation velocity increases due to collisions and the four-way coupling, and figures 27 and 28 show that the near-wall concentration decreases as mass loading increases. These trends are consistent with the trend of variation of the mean and fluctuation normal velocities observed, respectively, in figures 25, 26 and 15–17.

It is also of interest to evaluate the particle distribution in the channel, and in particular, to examine the effects of the two-way coupling and inter-particle collisions on preferential particle concentration. Figure 29(*a–d*) shows the locations of particles with $\tau^+ = 20$ superimposed on the vorticity contour at the channel

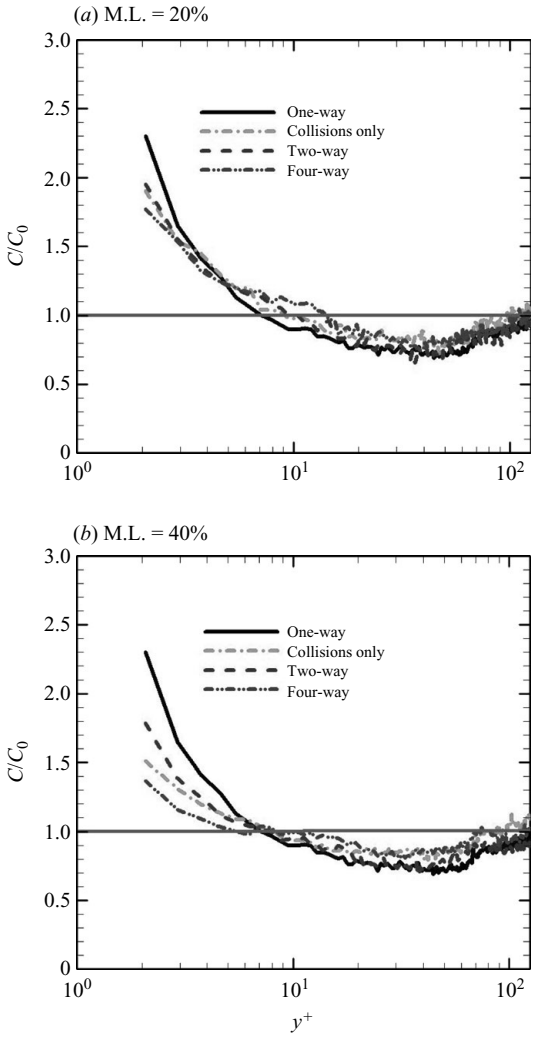

FIGURE 28. Particle concentration profile for different approaches, $\tau^+ = 20$, (*a*) ML = 20 % (*b*) ML = 40 %.

centreplane for different cases. It is observed that these inertial particles are responsive to the turbulent flow structures and are preferentially concentrated. In particular, the particles accumulate in regions of low vorticity. The observation that the particles appear to be flung out from regions of high vorticity into regions of low vorticity due to their inertia is consistent with the earlier works reported in the literature. Figure 29 also shows that the particle collisions and the two-way coupling slightly disperse the particles, but they do not noticeably change the particle preferential concentration at the channel centreplane.

Figure 30(*a–d*) shows the distribution of particles with $\tau^+ = 20$ for a mass loading of 40 % in the wall region at $y^+ = 10$ for different cases. The particles show strong preferential concentration patterns particularly for the one-way coupling case. Figure 30, however, shows that the inter-particle collisions and the two-way coupling significantly distort the particles' preferential concentration in the wall region.

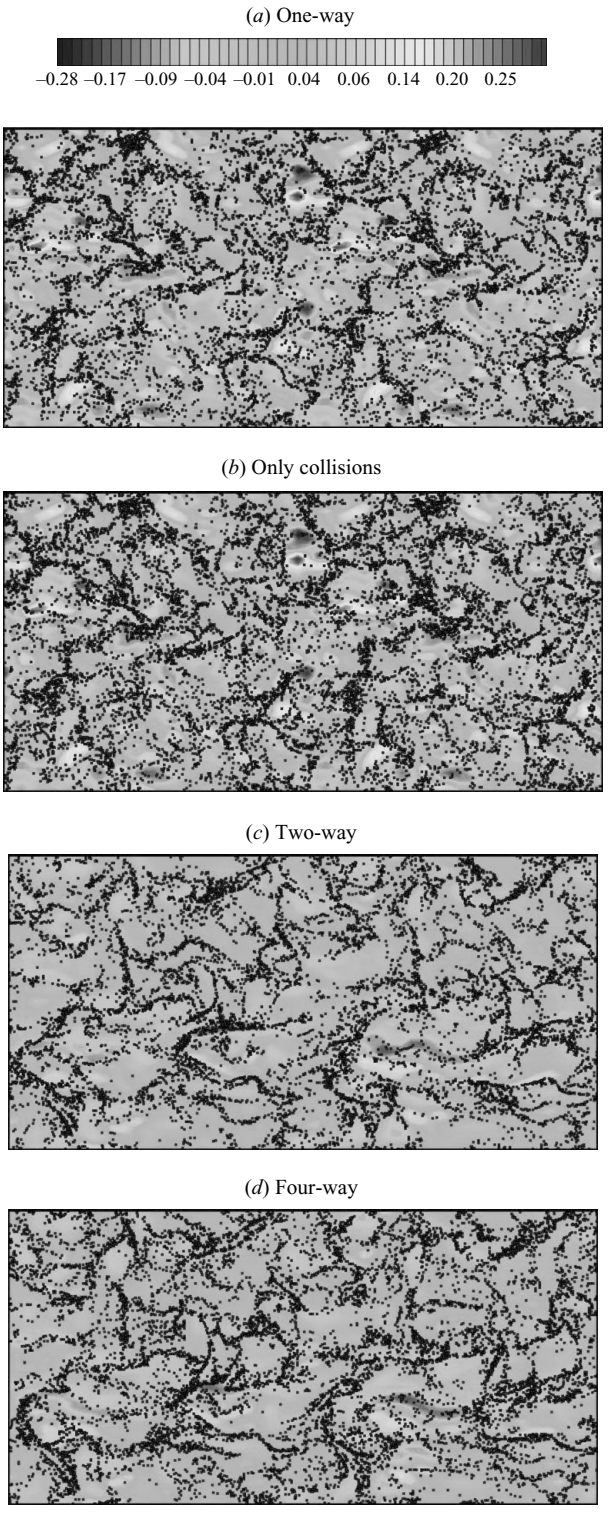

FIGURE 29. Distribution of $\tau_p^+ = 20$ particles for ML = 40 % at channel centreplane (*a*) one-way, (*b*) only collisions, (*c*) two-way, (*d*) four-way.

(*a*) One-way

(*b*) Only collisions

(*c*) Two-way

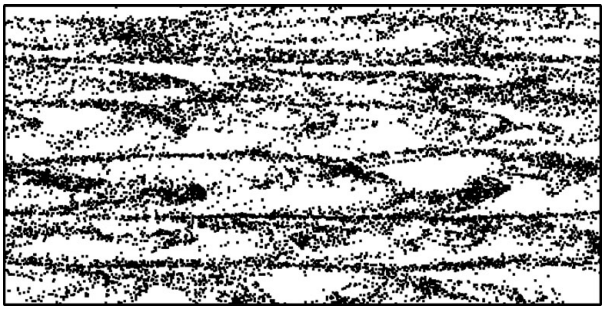

(*d*) Four-way

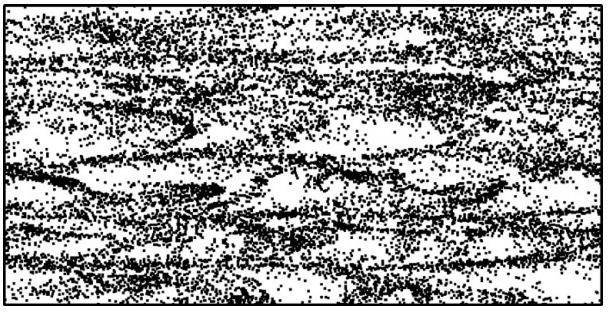

FIGURE 30. Distribution of $\tau_p^+ = 20$ particles for ML = 40 % at $y^+ = 10$ (*a*) one-way, (*b*) only collisions, (*c*) two-way, (*d*) four-way.

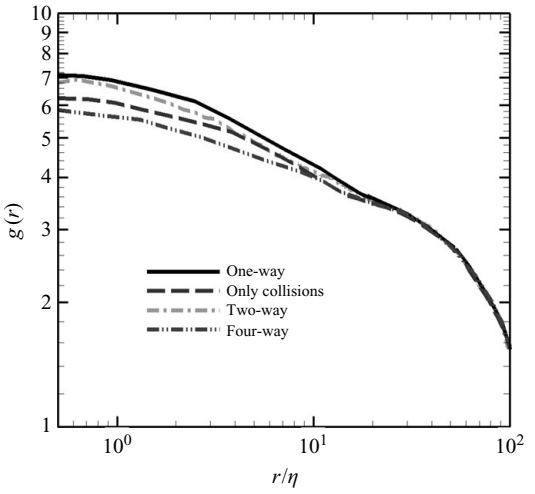

FIGURE 31. Two-dimensional radial distribution function, $g(r)$ vs. r/η for $\tau_p^+ = 20$ particles at ML = 40 %.

To quantitatively analyse the effect of the two-way coupling and inter-particle collisions on particle preferential concentration, we used the procedure introduced by Sundaram & Collins (1997) and evaluated the radial distribution functions for different cases. The radial distribution function gives the ratio of the number of particle pairs found at a given separation distance to the expected number of pairs if the particles are uniformly distributed.

The two-dimensional radial distribution function is defined as

$$g_{2D}(r_i) = \frac{P_i/A_i}{P/A}, \tag{19}$$

where P_i is the number of particle pairs with separation distances that lie between $r_i + \Delta r/2$ and $r_i + \Delta r/2$, $P = N_p(N_p - 1)/2$ is the total number of pairs, A is the total area of a planar slice and $A_i = \pi[(r_i + \Delta r/2)^2 - (r_i - \Delta r/2)^2]$ is the area of the shell associated with the nominal separation distance r_i within the plane.

Figure 31 shows the radial distribution function of $\tau^+ = 20$ particles in the wall region ($10 < y^+ < 12$) for different cases. As noted before, these particles exhibit preferential concentration due to interaction with the turbulent flow structures. The effect of the two-way coupling and inter-particle collisions can be clearly seen in figure 31. Note that both the two-way coupling and the inter-particle collisions reduce the particle clustering and the corresponding preferential concentration for this class of particles.

8. Conclusions

The effects of particle–particle collisions, the two-way coupling and the four-way coupling on particle deposition velocity, fluid and particle fluctuating velocity statistics and particle concentration profile in a turbulent channel flow were studied. The time history of the instantaneous turbulent velocity vector was generated by the two-way coupled DNS of the Navier–Stokes equation via a pseudo-spectral method. The particle equation of motion included the Stokes drag, the Saffman lift, and the gravitational forces. The effect of particles on the flow was included in the analysis via

a feedback force on the grid points. The key findings of the study may be summarized as follows:

(i) For the size ranges considered, the addition of particles attenuates the intensity of fluid turbulence fluctuations, and as particle mass loading increases, the level of attenuation increases.

(ii) Inter-particle collisions increase the particle Reynolds number, while the two-way coupling decreases it. In the case of the four-way coupling, the particle Reynolds number decreases compared with the one-way coupling case.

(iii) Inter-particle collisions increase the RMS particle normal fluctuating velocity, while the two-way coupling decreases it. In the case of the four-way coupling, the RMS particle normal fluctuating velocity decreases in the region where $y^+ > 10$ and increases in the wall region ($y^+ < 10$). At higher mass loading, the effect is magnified.

(iv) The two-way coupling causes a decrease in the number of deposited particles, while inter-particle collisions lead to an increase in the number of deposited particles. The increase in the number of deposited particles due to inter-particle collisions is larger than the decrease caused by the two-way coupling effects. Thus, for the physical case, the number of deposited particles increases with mass loading.

(v) Inter-particle collisions increase the particle deposition velocity as mass loading increases, while the two-way coupling decreases it. In the physical case (the four-way coupling), the particle deposition velocity increases compared with the one-way coupling case.

(vi) The four-way coupling decreases the particle normal fluctuating velocity, v'^p, in the $y^+ > 10$ region and increases it in the wall region with $y^+ < 10$ compared with the one-way coupling case. The two-way coupling effects decrease the particle normal fluctuating velocity, while inter-particle collisions enhance it.

(vii) The two-way coupling decreases the particle spanwise fluctuating velocity, w'^p, compared with the one-way coupling case as the particle mass loading increases, while inter-particle collisions enhance it as the particle mass loading increases. In the case of the four-way coupling, the particle spanwise fluctuating velocity decreases in the region with $y^+ > 4$ and increases very close to the wall ($y^+ < 4$) compared with the one-way coupling case.

(viii) The two-way coupling causes a decrease in particle streamwise fluctuating velocity, $\boldsymbol{u}'^p$, compared with the one-way coupling case. As particle mass loading increases, the level of attenuation in particle streamwise fluctuating velocity increases. Inter-particle collisions slightly enhance w'^p near the wall, but have no considerable effects in the channel core region. In the case of the four-way coupling, the particle streamwise fluctuating velocity decreases as particle mass loading increases compared with the one-way coupling case.

(ix) Inter-particle collisions decrease the particle mean normal velocity, $\bar{v}^{p^+}$, in the region where $y^+ > 5$, and increase it in the wall region, while the two-way coupling decreases it in the entire channel. In the case of the four-way coupling, the decrease in $\bar{v}^{p^+}$ is higher than the decrease in the case of the two-way coupling for the $y^+ > 5$ region.

(x) Both two-way coupling and inter-particle collisions reduce the concentration of particles near the wall. Therefore, in the four-way coupling case, in which both two-way coupling and inter-particle collisions are taken into account, the minimum particle accumulation near the wall is observed. Increasing particle mass loading intensifies the effects leading to a larger decrease in particle accumulation near the wall.

(xi) Particle–particle collisions and the two-way coupling reduce the preferential distribution of particles.

(xii) For the range of parameters studied in this work for inertial particles in a gas flow, no significant changes in the mean fluid and particle velocities, and the fluid and particle fluctuating velocities due to the particle aerodynamic interactions were observed. It is conceivable that for higher particle mass loadings (more than 100 %) or for liquid–solid flows this effect becomes important.

We gratefully acknowledge the financial support of the Environmental Protection Agency (EPA) and the NYSTAR Center of Excellence. We also thank the reviewers for their helpful suggestions.

REFERENCES

Arcen, B., Taniére, A. & Oesterle, B. 2006 On the influence of near-wall forces in particle-laden channel flows. *Intl J. Multiphase Flow* **32**, 1326–1339.

Ardekani, A. M. & Rangel, R. H. 2006 Unsteady motion of two solid spheres in Stokes flow. *Phys. Fluids* **18** (103306), 1–14.

Ayala, O., Grabowski, W. W. & Wang, L. P. 2007 A hybrid approach for simulating turbulent collisions of hydrodynamically-interacting particles. *J. Comput. Phys.* **225**, 51–73.

Beard, K. V. & Pruppacher, H. R. 1971 A wind tunnel investigation of the rate of evaporation of small water drop falling at terminal velocity in air. *J. Atmos. Sci.* **28**, 1455–1464.

Brooke, J. W., Kontomaris, K., Hanratty, T. J. & McLaughlin, J. B. 1992 Turbulent deposition and trapping of aerosols at a wall. *Phys. Fluids* A **4**, 825–834.

Caporaloni, M., Tampieri, F., Trombetti, F. & Vittori, O. 1975 Transfer of particles in nonisotropic air turbulence. *J. Atmos. Sci.* **32**, 565–568.

Caraman, N., Boree, J. & Simon, O. 2003 Effects of collisions on the dispersed phase fluctuation in a dilute tube flow: experimental and theoretical analysis. *Phys. Fluids* **15**, 3602–3612.

Chen, M., Kontomaris, K. & McLaughlin, J. B. 1997*a* Direct numerical simulation of droplet collisions in a turbulent channel flow-I. Collision algorithm. *Intl J. Multiphase Flow* **24**, 1079–1103.

Chen, M., Kontomaris, K. & McLaughlin, J. B. 1997*b* Direct numerical simulation of droplet collisions in a turbulent channel flow-II. Collision rate. *Intl J. Multiphase Flow* **24**, 1105–1138.

Chen, M. & McLaughlin, J. B. 1995 A new correlation for the aerosol deposition rate in vertical ducts. *J. Colloid Interface Sci.* **169**, 437–455.

Cleaver, J. W. & Yates, B. 1975 A sublayer model for deposition of the particles from turbulent flow. *Chem. Engng Sci.* **30**, 983.

Clift, R., Grace, J. R. & Weber, M. E. 1978 *Bubbles, Drops and Particles.* Academic Press.

Elghobashi, S. & Truesdell, G. C. 1993 On the two-way interaction of particle dispersion in a decaying isotropic turbulence. *Phys. Fluids* A **5**, 1790–1801.

Fan, F. G. & Ahmadi, G. 1993 A sublayer model for turbulent deposition of particles in vertical ducts with smooth and rough surfaces. *J. Aerosol Sci.* **24**, 45.

Fessler, J. R. & Eaton, J. K. 1994 Turbulence modification by particles in a backward facing step. *J. Fluid Mech.* **394**, 97–117.

Friedlander, S. K. & Johnstone H. F. 1957 Deposition of suspended particles from turbulent gas streams. *Ind. Engng Chem.* **49**, 1151–1156.

Hadinoto, K., Jones, E. N., Yurteri, C. & Curtis, J. S. 2005 Reynolds number dependence of gas-phase turbulence in gas-particle flows. *Intl J. Multiphase Flow* **31**, 416–434.

He, C. & Ahmadi, G. 1999 Particle deposition in a nearly developed turbulent duct flow with electrophoresis. *J. Aerosol Sci.* **30**, 739.

Hetsroni, G. & Sokolov, M. 1971 Distribution of mass, velocity and intensity of turbulence in a two-phase turbulence jet. *Trans. ASME J. Appl. Mech.* **38**, 315–327.

Kulick, J. D., Fessler, J. R. & Eaton, J. K. 1994 Particle response and turbulence modification in fully developed channel flow. *J. Fluid Mech.* **277**, 109–134.

Levy, Y. & Lockwood, F. C. 1981 Velocity measurements in a particle-laden turbulence free jet. *Combust. Flame* **40**, 333–339.

Li, A. & Ahmadi, G. 1992 Computer simulation of deposition of aerosols in a turbulent channel flow with rough wall. *Aerosol Sci. Technol.* **16**, 209.

Li, Y., McLaughlin, J. B., Kontomaris, K. & Portela, L. 2001 Numerical simulation of particle-laden turbulent channel flow. *Phys. Fluids.* **13** (10), 2957–2967.

Marchioli, C. & Soldati, A. 2002 Mechanisms for particle transfer and segregation in a turbulent boundary layer. *J. Fluid Mech.* **468**, 283–315.

McLaughlin J. B. 1989 Aerosol particle deposition in numerically simulated turbulent channel flow. *Phys. Fluids* A **1**, 1211.

McLaughlin, J. B. 1994 Numerical computation of particle–turbulence interaction. *Intl J. Multiphase Flow* **20** (Suppl.), 211–232.

Narayanan, C., Lakehal, D., Botto, L. & Soldati, A. 2003 Mechanisms of particle deposition in a fully developed turbulent open channel flow. *Phys. Fluids* **15** (3), 763–775.

Nasr, H. & Ahmadi, G. 2007 The effect of two-way coupling and inter-particle collisions on turbulence modulation in a vertical channel flow. *Intl J. Heat Fluid Flow* **28** (6), 1507–1517.

Ounis, H., Ahmadi, G. & McLaughlin, J. B. 1991 Dispersion and deposition of Brownian particles from point sources in a simulated turbulent channel flow. *J. Colloid Interface Sci.* **147**, 233.

Ounis, H., Ahmadi, G. & McLaughlin, J. B. 1993 Brownian particle deposition a directly simulated turbulent channel flow. *Phys. Fluids* A **5**, 1427.

Papavergos, P. G. & Hedley, A. B. 1984 Particle deposition behaviour from turbulent flows. *Chem. Engng Res. Des.* **62**, 275–295.

Portela, L. M. & Oliemans, R. V. A. 2003 Eulerian–Lagrangian DNS/LES of particle–turbulence interactions in wall-bounded flows. *Intl J. Numer. Meth. Fluids* **43**, 1045–1065.

Rashidi, M., Hetsroni, G. & Banerjee, S. 1990 Particle–turbulence interaction in a boundary layer. *Intl J. Multiphase Flow* **16**, 935–949.

Reeks, M. W. 1983 The transport of discrete particles in inhomogeneous turbulence. *J. Aerosol Sci.* **14**, 729–739.

Squires, K. D. & Eaton J. K. 1990 Particle response and turbulence modification in isotropic turbulence. *Phys. Fluids* A **2**, 1191–1203.

Squires, K. D. & Eaton, J. K. 1991*a* Measurements of particle dispersion obtained from direct numerical simulations of isotropic turbulence. *J. Fluid Mech.* **226**, 1–35.

Squires, K. D. & Eaton J. K. 1991*b* Preferential concentration of particles by turbulence. *Phys. Fluids* A **3**, 1169–1178.

Sundaram, S. & Collins, L. R. 1997 Collision statistics in an isotropic particle-laden turbulent suspension. Part 1. Direct numerical simulations. *J. Fluid Mech.* **335**, 75–109.

Tsuji, Y. & Morikawa, Y. 1982 LDV measurements of an air–solid two-phase flow in a horizontal pipe. *J. Fluid Mech.* **226**, 385–409.

Tsuji, Y., Morikawa, Y. & Shiomi, H. 1984 LDV measurements of an air–solid two-phase flow in a vertical pipe. *J. Fluid Mech.* **139**, 417–434.

Vreman, A. W. 2007 Turbulence characteristics of particle-laden pipe flow. *J. Fluid Mech.* **584**, 235–279.

Wang, L. P. & Stock, D. E. 1993 Dispersion of heavy particles by turbulent motion. *J. Atmos. Sci.* **50**, 1897–1913.

Wang, Q. & Squires, K. D. 1996 Large eddy simulation of particle-laden turbulent channel flow. *Phys. Fluids* **8** (5), 1207–1223.

Wood, N. B. 1981 A simple method for calculation of turbulent deposition to smooth and rough surfaces. *J. Aerosol Sci.* **12**, 275.

Yamamoto, Y., Potthoff, M., Tanaka, T., Kajishima, T. & Tsuji, Y. 2001 Large eddy simulation of turbulent gas–solid flow in a vertical channel: effect of considering inter-particle collisions. *J. Fluid Mech.* **442**, 303–334.

Yarin, L. P. & Hetsroni, G. 1994 Turbulence intensity in dilute two-phase flow. 3. The particles–turbulence interaction in dilute two-phase flow. *Intl J. Multiphase Flow* **20**, 27–44.

Young, J. & Leeming, A. 1997 A theory of particle deposition in turbulent pipe flow. *J. Fluid Mech.* **340**, 129–159.

Zhang, H. & Ahmadi, G. 2000 Aerosol particle transport and deposition in vertical and horizontal turbulent duct flows. *J. Fluid Mech.* **406**, 55–80.